

Catalysis Science & Technology

Accepted Manuscript



This is an *Accepted Manuscript*, which has been through the Royal Society of Chemistry peer review process and has been accepted for publication.

Accepted Manuscripts are published online shortly after acceptance, before technical editing, formatting and proof reading. Using this free service, authors can make their results available to the community, in citable form, before we publish the edited article. We will replace this *Accepted Manuscript* with the edited and formatted *Advance Article* as soon as it is available.

You can find more information about *Accepted Manuscripts* in the [Information for Authors](#).

Please note that technical editing may introduce minor changes to the text and/or graphics, which may alter content. The journal's standard [Terms & Conditions](#) and the [Ethical guidelines](#) still apply. In no event shall the Royal Society of Chemistry be held responsible for any errors or omissions in this *Accepted Manuscript* or any consequences arising from the use of any information it contains.



Journal Name

ARTICLE

A comprehensive approach to investigate the structural and surface properties of activated carbons and related Pd-based catalysts

Received 00th January 20xx,
Accepted 00th January 20xx

DOI: 10.1039/x0xx00000x

www.rsc.org/

A. Lazzarini,^a A. Piovano,^{b,*} R. Pellegrini,^c G. Leofanti,^d G. Agostini,^e S. Rudić,^f M. R. Chierotti,^a R. Gobetto,^a A. Battiato,^g G. Spoto,^a A. Zecchina,^a C. Lamberti^{a,h} and E. Groppo^{a,*}

Activated carbons are widely used as supports for industrial catalysts based on metal nanoparticles. The catalytic performances of carbon-supported catalysts are strongly influenced by the carbon activation method. Notwithstanding this important role, the effect induced by different activation methods has been rarely investigated in details. This work deals with two carbons of wood origin, activated either by steam or by phosphoric acid, and the corresponding catalysts based on supported Pd nanoparticles. We demonstrate that the catalysts perform in a different way in hydrogenation reactions depending to the nature of the carbon used as a support, being the palladium dispersion the same. We propose a multi-technique approach to fully characterize both carbons and catalysts at the micro- and at the nanoscale. In particular, we investigate how the activation procedure influences the texture (by N₂ physisorption), the morphology (by Scanning Electron Microscopy), the structure (by Solid State Nuclear Magnetic Resonance, Raman spectroscopy and X-Ray Diffraction) and the surface properties (by X-ray Photoelectron spectroscopy, Diffuse Reflectance Infrared Spectroscopy and Inelastic Neutron Scattering) of carbons and of the related catalysts. The comprehensive characterization approach proposed in this work allows to rationalize, at least in part, the role of activated carbons in enhancing the performances of a hydrogenation catalyst.

1. Introduction

Activated carbons are important modifications of carbon that find a wide use in the field of catalysis, where they are usually employed as supports for noble metal nanoparticles. They consist of carbonized bio-polymeric materials activated in a second step of the synthesis process.¹⁻³ A large number of patents describe numerous ways to activate carbon from several natural sources, such as wood, peat or coconut shells.¹⁻⁷ Activation is usually performed in the presence of steam, or by adding phosphoric acid to the raw product, resulting in activated carbons having different properties in terms of porosity, structure at a micro- and nano-scale, and surface

chemistry. All these three factors play a fundamental role in catalysis. The support may have a direct influence on the catalytic reaction, because its surface is often active toward reactants and reaction products.⁸ In addition, the support may exhibit an indirect influence, because its physical-chemical properties may affect the properties of the deposited metal nanoparticles (such as shape, size distribution and dispersion), their tendency to aggregate under catalytic conditions (i.e. resistance to sintering), and the accessibility of active sites to reactants.^{1-3,9-13}

Pore size and pore volume are important factors for physical adsorption. Many works in the literature report detailed analysis of the porosity of carbons activated following different routes.^{5,7,14} It is now well established that in all cases a high specific surface area is obtained (up to 1500 m²·g⁻¹), due to the oxidative generation of micro-pores of variable size and shape distribution. In presence of phosphoric acid, a fraction of the additive is incorporated during carbonization into the carbon body, and is subsequently removed by leaching; as a consequence, this procedure generally creates pores having a pore size distribution narrower with respect to those obtained by oxidation in steam.¹⁵ In terms of local structure, an activated carbon is usually described as constituted by significant amounts of graphite-like (or sp²) species depending on the temperature of activation.¹⁶ Although all of them are characterized by the same predominant structural unit, activated carbons may differ in terms of their nano-structure,

^a Department of Chemistry, NIS Centre and INSTM, University of Turin, Via Giuria 7, I-10125, Turin, Italy. E-mail: elena.groppo@unito.it

^b Institut Laue-Langevin (ILL), 71 avenue des Martyrs, 38000 Grenoble, France. E-mail: piovano@ill.fr

^c Chimet SpA - Catalyst Division, Via di Pescaiola 74, Viciomaggio Arezzo, I-52041 Italy.

^d Consultant, Via Firenze 43, 20010 Canegrate, Milano, Italy.

^e European Synchrotron Radiation Facility (ESRF), 71 avenue des Martyrs, 38000 Grenoble, France.

^f ISIS Facility, Rutherford Appleton Laboratory, Chilton, Didcot, Oxfordshire, OX11 0QX, UK.

^g Department of Physics, NIS Centre, University of Turin, Via Giuria 1, I-10125, Turin, Italy.

^h Southern Federal University, Zorge street 5, 344090 Rostov-on-Don, Russia.

† Electronic Supplementary Information (ESI) available: [The chemical composition of the two carbons determined by EDX analysis, ¹H CPMAS NMR spectra of the two carbons]. See DOI: 10.1039/x0xx00000x

that means the connectivity of the sp^2 domains from molecular dimensions up to a few nanometers. Finally, the surface chemistry of carbons plays a key role in specific adsorption and is relevant to all aspects of catalysis. The two most important hetero-elements are hydrogen and oxygen, each of which can undergo a variety of chemically different coordination geometries, creating a rich surface chemistry. Hydrogen is naturally present in activated carbons to terminate the sp^2 domains. In addition, it is well documented that a large number of oxygen functional groups are created during the activation process by the saturation of dangling bonds with oxygen.^{17,18}

It is evident that activated carbons as catalyst supports (but also as catalysts in their own) offer incomparable flexibility in tailoring catalysts properties to specific needs. However, a comprehensive characterization of the structural and surface properties of activated carbons is fundamental to understand their role in catalysis. Activated carbons have been widely investigated in the literature.¹⁻³ Conflicting information are often found, along with highly fragmented results, mainly as a consequence of an uncritical use of different methodologies. Due to the intrinsic complexity of activated carbons, no single technique is able to give a complete picture of the overall properties of activated carbons; instead, a range of complementary characterization techniques is needed to characterise these materials at different dimension scales.

In this work we investigate in detail two activated carbons and the corresponding Pd/C catalysts. The two carbons are originated from the same raw material (wood), but have been activated either by steam (C_W) or by phosphoric acid (C_{Chem}). At first, we explore the catalytic performances of Pd/C catalysts in hydrogenation reactions, as a function of the activated carbon used as a support. Then, we systematically characterize the morphological, structural and surface properties of the two activated carbons and of the related catalysts, by means of a multi-technique approach. In particular, we apply N_2 physisorption to evaluate surface area and porosity, Scanning Electron Microscopy (SEM) to investigate the morphology at a micrometric scale, X-ray Powder Diffraction (XRPD), 1H and ^{13}C Solid-State Nuclear Magnetic Resonance (SSNMR) and Raman spectroscopy to determine the structural properties at the nanometric scale, X-ray Photoelectron spectroscopy (XPS), Diffuse Reflectance Infrared Fourier-Transformed (DRIFT) and Inelastic Neutron Scattering (INS) spectroscopies to investigate the surface properties. Although some of these techniques are commonly applied to investigate carbon-based materials, to the best of our knowledge this is the first time that such a large number of characterization techniques are simultaneously used to investigate the same activated carbons and related catalysts. In particular, to the best of our knowledge, no other work reports the synergic combination of Raman, DRIFT and INS spectroscopies to achieve a full vibrational characterization of carbon-based materials.

2. Experimental section

2.1 Materials

Two commercial grades of activated carbons, both having wood origin, were provided by Chimet S.p.A.¹⁹ C_W is activated at high temperature in the presence of steam, whereas C_{Chem} is activated at high temperature after impregnation with phosphoric acid.

Pd/C catalysts (metal loading of 5.0 wt%) were prepared in the Chimet Laboratories on C_W and C_{Chem} carbons, following the deposition-precipitation method as reported elsewhere.⁹ Na_2PdCl_4 was used as the palladium precursor and Na_2CO_3 as the basic agent. All the catalysts were water-washed until residual chlorides were removed, and dried at 120 °C overnight. No metal was found in the solution after filtration (as determined by ICP). In some cases, pre-reduction was carried out before washing with formate at 65 °C for 1 h.²⁰ Hereafter, Pd/ C_W and Pd/ C_{Chem} will be used to indicate the unreduced Pd-based catalysts prepared on C_W and C_{Chem} carbons, respectively. When a pre-reduction is performed, a label indicating the reducing agent is added. Thus, Pd/ C_W (F) and Pd/ C_{Chem} (F) refer, respectively, to C_W and C_{Chem} supported palladium catalysts (5.0 wt % loading) reduced with formate.

2.2 Catalytic performances in hydrogenation reactions

The catalytic performances of the Pd/C catalysts were tested in a transfer hydrogenation²¹ and a debenzilation reaction.²² Transfer hydrogenation of resorcinol to 1,3-cyclohexanedione²³ was carried out in a 300 cm³ glass reactor equipped with a double mantle for water circulation, and magnetic stirrer, a gas inlet and a reflux condenser. Water at the required temperature was circulated inside the reactor mantle by means of a circulation bath. Reactor was charged with 125 ml of water, 55.0 g of resorcinol and 44.2 g of sodium formate. The reaction mixture was heated to 40 °C while stirring and purging the reaction medium with nitrogen gas for 30 minutes. Then, 2.75 g of Pd/C catalyst were added and held for 3 hours. After that, the temperature was raised at 55 °C and maintained for 15 hours. Samples have been withdrawn at 2, 3, and 18 hours and analysed by HPLC to determine conversion and selectivity.

Debenzilation of N-benzyl-N-ethylaniline to N-ethylaniline and toluene²⁴ was carried out in a 500 cm³ autoclave equipped with a heating mantle, mechanical stirrer and gas regulation system able to perform the reaction at constant pressure. The autoclave was charged with 300 ml of ethanol, 150 g of N-benzyl-N-ethylaniline and 3.0 g of Pd/C catalyst. The autoclave was closed and purged first with nitrogen and then with hydrogen. Hydrogenation was performed at a temperature of 65°C, a pressure of 3 bar and a stirring speed of 900 rpm. The automatic recording of the hydrogen consumption allowed to plot the consumption curve and then the catalytic activity expressed in mmol H_2 /min g_{cat}.

2.3 Methods

N_2 physisorption – The surface area and pore volume of carbons were measured by N_2 physisorption at 77 K.

Measurements were performed on a Micromeritics ASAP 2020 instrument. The adsorption isotherm were analysed according to the procedure described in Ref⁹.

SEM - SEM images were collected at 20 kV of voltage with a Zeiss EVO MA10 instrument equipped with LaB6 filament. The samples were put on an Al stub covered with a double-layer adhesive disk. EDX analysis has been performed with OXFORD x-act detector using AztecEnergy analysis software.

XRPD - X-ray Powder Diffraction patterns were collected with a PW3050/60 X'Pert PRO MPD diffractometer from PANalytical working in the Debye-Scherrer geometry, using as a source a Cu anode filtered by a Ni foil to attenuate the $K\beta$ line and focused by a PW3152/63 X-ray mirror ($\lambda = 1.5409 \text{ \AA}$). The samples were measured as powders in a glass capillary. The average dimension (L_a) of the crystalline domains has been obtained by applying the Scherrer equation, $L_a = K\lambda/\beta\cos(\theta_{\text{Bragg}})$, where λ is the wavelength of the Cu K_α radiation (1.541 \AA), K the shape factor (fixed to 0.9),²⁵ and β is the FWHM (in 2θ , corrected by the instrumental broadening) of the (100) and (110) reflections.

SSNMR spectroscopy - SSNMR spectra were recorded on a Bruker Avance II 400 instrument operating at 400.23, 162.02 and 100.65 MHz for ^1H , ^{31}P and ^{13}C nuclei, respectively. Cylindrical 4 mm of diameter zirconia rotors with a sample volume of 80 μl were employed and spun at 12 kHz. All CPMAS experiments employed the Ramp-Amplitude Cross-Polarization pulse sequence (^1H 90° pulse = 3.05 μs , contact time = 1.5 ms, relaxation delay 0.2 s) with the Two Pulse Phase Modulation ^1H decoupling with an rf field of 75 kHz during the acquisition period. ^1H MAS experiments were performed on 2.5 mm probe. The rotors (12 μl volume) were spun at 32 kHz. A DEPTH sequence ($\pi/2-\pi-\pi$) for the suppression of the probe background signal was used. ^1H , ^{13}C and ^{31}P chemical shifts were referenced with the resonance of adamantane (^1H signal at 1.87 ppm), glycine (^{13}C methylene signal at 43.86 ppm) and 85% phosphoric acid (^{31}P signal at $\delta = 0$ ppm) as external standards.

XPS spectroscopy - The XPS measurements were performed in a ultrahigh vacuum (1×10^{-7} Pa) system equipped with a VSW Class 100 Concentric Hemispherical Analyzer. The samples were mounted on a copper tape, opportunely degassed and transferred into the analysis chamber. A non-monochromatic Al K_α (VSW TA10) X-ray source of incident energy of 1486.6 eV was applied to generate core excitation. The energy step at the survey spectra was 1 eV, while the energy step at the C 1s spectra was 0.2 eV. Two different modes were employed in the XPS measurements: low resolution (fixed analyzer transmission at a pass energy of 44 eV, FAT 44) for survey spectra and high resolution (fixed analyzer transmission at a pass energy of 22 eV, FAT 22) for core lines scans and quantitative surface composition.

The XPS analysis depth in case of carbon matrix is about 10 - 15 nm. The spectra were analysed and processed with the use of Unifit2008© software. The background was approximated by a third order polynomial function combined with the Shirley model for inelastic processes, and the detailed spectra were fitted with a convolution of gaussian functions.

DRIFT spectroscopy - DRIFT spectra were collected on a Nicolet 6700 instrument equipped with a ThermoFisher Smart accessory and an MCT detector, at 4 cm^{-1} resolution and averaging 1024 scans. The measurements were performed on powdered samples in air, without dilution in KBr. The spectra were collected in reflectance and successively converted in Kubelka-Munk units (K.M.).

Raman spectroscopy - Raman spectra were recorded by using a Renishaw inVia Raman microscope instrument, with an excitation $\lambda = 514 \text{ nm}$. The laser power was fixed at 0.5 % of the total, after having checked the sample stability under the laser beam. The photons scattered by the sample were dispersed by a 1800 lines/mm grating monochromator and simultaneously collected on a CCD camera; the collection optic was set at 20X objective. The spectra were obtained by collecting 20 acquisitions (each of 50 s) on samples in the powder form. UV-Raman spectra were collected with a Renishaw Micro-Raman System 1000 equipped with a frequency doubled Ar^+ laser, operating at 244 nm. The laser power was adjusted to avoid carbon degradation. The photons scattered by the sample were dispersed by a 3600 lines/mm grating and simultaneously collected by a CCD detector; the collection optic was set at 15X objective. The spectra were obtained by collecting 10 acquisitions (each of 30 s) on samples in the powder form.

INS spectroscopy - The INS spectra were recorded at the TOSCA spectrometer at ISIS spallation neutron source (Rutherford Appleton Laboratory, UK).²⁶ The samples were previously treated in vacuum at 150 °C for a prolonged time in order to remove the physisorbed water. Successively, they were inserted in a thin aluminium envelope and then placed into In-wire sealed Al cells. All the manipulations were performed inside a glove-box to prevent contamination by moisture. Finally, the cell was inserted in a duplex CCR cryostat, and the measurements were performed at 20 K. Each INS spectrum was measured with a high statistic, by integrating for 1500 μA of the proton current (proton accelerator was working at about 150 $\mu\text{A}/\text{hour}$). The signal from detectors both in forward and in backward directions have been extracted and combined using Mantid software,²⁷ without any sign of degradation of the resolution. The beam size was 40 mm x 40 mm so that a representative macroscopic amount (7.706 g for C_w and 7.650 g for C_{chemi}) of samples were measured in each experiment. Since the intensity of the INS signal is proportional to the amount of the corresponding chemical species, the spectra were normalized on sample mass and incoming proton current values in order to allow a quantitative comparison among the samples.

CO chemisorption - The metal dispersion for Pd/C catalysts was evaluated by means of CO chemisorption method. CO chemisorption measurements were performed at 50 °C by a dynamic pulse method on samples pre-reduced in H_2 at 120 °C.²⁸ In a typical experiment, the catalyst (200 mg) is loaded inside the U-tube, heated in He up to 120 °C (heating rate of $10 \text{ }^\circ\text{C min}^{-1}$), reduced in H_2 for 30 min, and finally cooled down to 50 °C in He (cooling rate of $10 \text{ }^\circ\text{C min}^{-1}$). A CO/metal

average stoichiometry of 1 was assumed to calculate the metal dispersion, as widely documented.^{29,30}

3. Results and Discussion

3.1 Catalytic performances of Pd/C catalysts in hydrogenation reactions

The catalytic performances of the Pd/C catalysts in two selective hydrogenation reactions are summarized in Table 1 and Table 2. The pre-reduced Pd/C_W(F) and Pd/C_{Chem}(F) catalysts were tested in the transfer hydrogenation of resorcinol to 1,3-cyclohexanedione using sodium formate as the hydrogen source (Chart 1 and Table 1). Although the two catalysts have a similar metal dispersion and display a similar conversion as a function of time, they give a different selectivity to 1,3-cyclohexanedione. In particular, Pd/C_W(F) is more selective than Pd/C_{Chem}(F), reaching almost 100% of selectivity at full conversion.

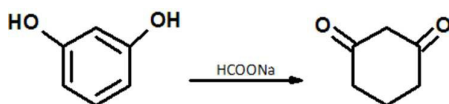


Chart 1.

Table 1. Catalytic performances of Pd/C_W(F) and Pd/C_{Chem}(F) catalysts in the hydrogenation of resorcinol with formate. Reaction conditions: T = 40 – 55 °C, 5 wt% catalyst loading. D (%) indicates the palladium dispersion as evaluated by CO chemisorption method. Selectivity value is referred at 18 h.

Catalyst	D (%)	Conversion (%)			Selectivity (%)
		2 h	3 h	18 h	
Pd/C _W (F)	28.1	30.8	40.2	96.2	98.82
Pd/C _{Chem} (F)	26.3	29.4	38.1	96.8	85.16

The unreduced Pd/C_W and Pd/C_{Chem} catalysts were tested in the debenzylation of N-benzyl-N-ethylaniline to give N-ethylaniline and toluene (Chart 2 and Table 2). Also in this case the metal dispersion is quite similar for the two catalysts, but Pd/C_{Chem} is much more active than Pd/C_W.

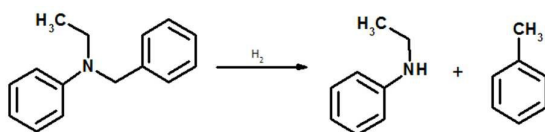


Chart 2.

Table 2. Catalytic performances of Pd/C_W and Pd/C_{Chem} catalysts in the debenzylation of N-benzyl-N-ethylaniline to give N-ethylaniline and toluene. Reaction conditions: T = 65 °C, P = 3 bar, 3 wt% catalyst loading. D (%) indicates the palladium dispersion as evaluated by CO chemisorption method.

Catalyst	D (%)	Activity (mmol H ₂ /min g _{cat})
Pd/C _W	23.5	14.6
Pd/C _{Chem}	18.8	31.1

These data clearly demonstrate that the catalytic performances (in terms of both activity and selectivity) of Pd/C catalysts in hydrogenation reactions are strongly affected by the nature of the support, being the palladium dispersion similar in the two couples of catalysts. This is well known in the industrial practice, but the reasons were never investigated in a systematic way. In most of the cases only the metal phase was characterized in detail, whereas very little attention was devoted to the investigation of the support properties, especially when dealing with carbons whose “black” nature makes the characterization techniques using IR, visible and near UV photons not straightforwardly applicable.³¹⁻³³

3.2 Chemical composition, morphology and porous texture of C_W and C_{Chem}

The average composition of C_W and C_{Chem} was determined by means of Electron Dispersive X-ray (EDX) analysis (Table S1), by averaging the measurements performed on five different carbon granules. Complementary information on the surface composition were obtained by XPS spectroscopy (Fig. S1, Table S2 and Table S3). Both carbons contain a substantial amount of oxygen, which is at least in part contained in inorganic insoluble ashes. The ash content in the two carbons was quantitatively determined by calcination, and resulted in 0.58 wt% for C_W and 1.96 wt% for C_{Chem}. Compositional analysis indicates that they are mainly composed of silico-aluminates. Accordingly, Si is detected by XPS in C_{Chem} and hardly visible in C_W. Phosphorous is also present in the inorganic ashes in C_{Chem} (see below). The role of the inorganic ashes in affecting the catalysts' performances is expected to be marginal because of their very low concentration.

In addition, C_{Chem} carbon contains a consistent amount of phosphorous, in agreement with recent literature reporting that activation with phosphoric acid not only develops porosity, but also leads to the inclusion of a significant amount of phosphorous into the carbon structure.³⁴⁻³⁷ The nature and localization of the phosphorous contained in C_{Chem} was clarified by ³¹P Cross-Polarization Magic Angle Spinning (CP-MAS) Solid-State Nuclear Magnetic Resonance (SSNMR) measurements and X-ray photoelectron spectroscopy. The ³¹P CPMAS NMR spectrum (Fig. S2) is characterized by two main signals, centred around 1.3 and 14.1 ppm. The former is characteristic of phosphates, i.e. phosphorus bound to four oxygen atoms, likely contained in the inorganic ashes. On the contrary, the resonance at 14.1 ppm is attributed to phosphonates, i.e. organo-phosphorous compounds containing one P-C bond, revealing that at least a fraction of phosphorous has functionalized the carbon.³⁴⁻³⁷ Interestingly, XPS measurements (Fig. S1) do not reveal the presence of phosphorous, indicating that it is not localized at the surface of C_{Chem}, and hence it is not relevant for catalysis. This is in contrast to the findings of Puziy et al.,³⁷ which however are related to chemically activated carbons of different origin (polymer- and fruit-stone-based carbons).

Fig. 1 shows a few representative SEM pictures of C_W (part a) and C_{Chem} (part b) carbons. In both cases, irregular micro-

particles are observed, which resemble the peculiar structures of the pristine wood. In particular, reminiscence of the original vascular bundles and tracheids are clearly observed in C_W (see inset in Fig. 1a), whereas they are hardly detectable for C_{Chemir} , which shows on average much smaller micro-particles. These morphological differences on a micro-scale are in good agreement with the average particle size as determined by light scattering, and reflect the harsher activation conditions for C_{Chemir} . It is expected that the different micro-structure has an influence on the macroscopic mechanical properties of the two carbons. Finally, the textural properties of the two carbons were investigated by means of N_2 physisorption at 77 K. Fig. 1c shows the N_2 physisorption isotherms collected at 77 K for C_W and C_{Chemir} carbons. The activation process substantially affects the textural properties of carbons. The specific surface area is approximately $1000 \text{ m}^2 \cdot \text{g}^{-1}$ for the C_W and $1500 \text{ m}^2 \cdot \text{g}^{-1}$ for C_{Chemir} , which also displays a significantly larger total pore volume.

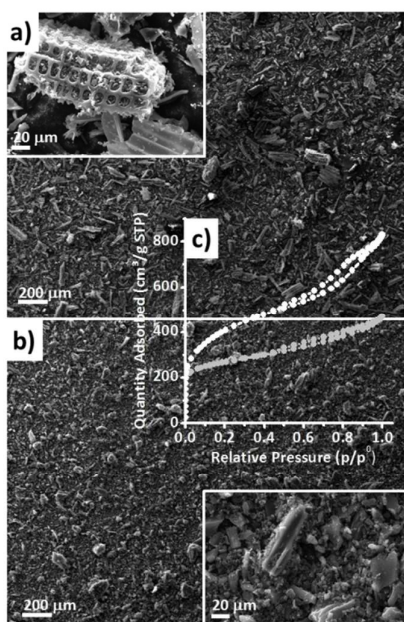


Fig. 1. Representative SEM images of C_W (part a) and C_{Chemir} (part b). Part c shows the N_2 physisorption isotherms collected at 77 K for C_W (grey) and C_{Chemir} (white).

3.3 Structural properties of C_W and C_{Chemir} at a nanometric scale

3.3.1 XRPD measurements. The structure of the two carbons at a nanometric scale was evaluated at first by means of XRPD technique. The XRPD patterns of both carbons (Fig. 2, inset) do not show distinct sharp diffraction peaks, but only three very broad peaks can be distinguished, more intense for C_W than for C_{Chemir} . These peaks resemble those typical of crystalline graphite, and demonstrate that both carbons are characterized by small graphitic islands, in agreement with literature data.^{16,38-41} To better appreciate the differences among the two carbons, the background was subtracted from the original patterns (main part of Fig. 2). The first peak (centred around $2\theta = 23^\circ$) corresponds to the (002) reflection

of graphite, which is attributed to the stacking of the graphene layers.^{16,39,40} The other two peaks (centred around $2\theta = 44^\circ$ and 80°) correspond to the (100) and (111) reflections originating from the in plane structure of graphitic crystallites.^{16,39,40} Narrower peaks correspond to crystallites having a larger lateral dimension. These peaks are narrower in the diffraction pattern of C_W , suggesting that on average the sp^2 islands are larger in C_W than in C_{Chemir} .

The lateral size (L_a) of the sp^2 -ordered crystallites has been estimated from the width of the (100) and (111) peaks by using the Scherrer equation, resulting in $L_a = 16.5 \pm 0.5 \text{ \AA}$ for C_W and $L_a = 12.5 \pm 0.5 \text{ \AA}$ for C_{Chemir} . However, it should be noticed that several discrepancies are reported in literature on the exact determination of the average crystallite size according to the different methods of peak profile evaluation and also that defects and strain within the carbon lattice would contribute to the diffraction broadening.^{16,42-44} For the present discussion, it is sufficient to notice that the activation procedure influences the in-plane dimension of the graphitic

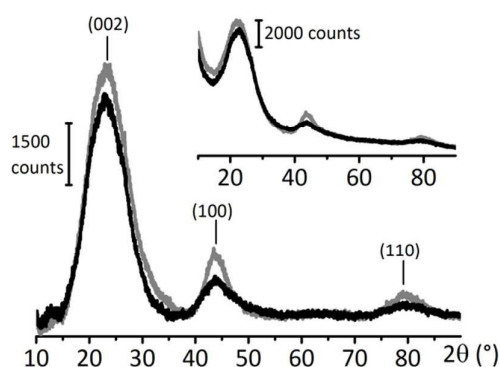


Fig. 2. XRPD patterns of C_W (grey) and C_{Chemir} (black) carbons after subtraction of the background, and assignment of the main peaks ($\lambda = 1.5409 \text{ \AA}$). The inset shows the patterns as collected.

domains in carbons. In particular, C_W is characterized, in average, by sp^2 crystallites larger than C_{Chemir} , but in both cases the lateral size of regular sp^2 islands is smaller than 2 nm. It is worth noticing that the presence of defects (such as heteroatoms) is sufficient to remove the aromaticity and hence to disrupt the regularity of the sp^2 domains.

3.3.2 ^1H and ^{13}C SSNMR measurements. The carbon local structure was investigated by ^{13}C CPMAS SSNMR measurements, which offer complementary information to the XRPD data discussed above. Indeed, it is well known that SSNMR techniques can provide structural information in materials that cannot be fully characterized using X-ray crystallography due to the lack of sufficient long range order.^{45,46} While diffraction experiments reveal topological data, SSNMR unravels connections and distances on local and intermediate length scales.⁴⁷ In this sense, it does not require the long range order needed by diffraction techniques. Furthermore, the usefulness of SSNMR stems also from its ability to non-destructively investigate multi-component and multi-phase systems at the bulk level.

The ^{13}C CPMAS NMR spectra of both C_W and C_Chemical carbons, shown in Fig. 3, are entirely dominated by a broad peak centered around 125 ppm, which is characteristic of sp^2 -hybridized carbon in condensed aromatic rings. The line width of the signal is much broader for C_W (FWHM = 3120 Hz) than for C_Chemical (FWHM = 1820 Hz). In principle, the observation of broad resonances can be related to the presence of paramagnetic impurities or a distribution of slightly different chemical environments typical of condensed aromatic carbon systems of different size. EPR spectra (not reported) reveal in both cases the presence of a very small amount of carbon-centred radicals (signals with g -value ~ 2.0033). Thus, from the very low density of carbon radicals in both samples, we can surmise that the broader resonance in the ^{13}C CPMAS NMR spectrum of C_W is associated with a larger distribution of sp^2 islands having a different size. In addition to the signal at 125 ppm, in the spectrum of C_Chemical a very weak peak is observed around 180 ppm (inset in Fig. 3), which is indicative of the presence of a small amount of oxygen-containing surface functional groups. Although the band is weak and broad, its

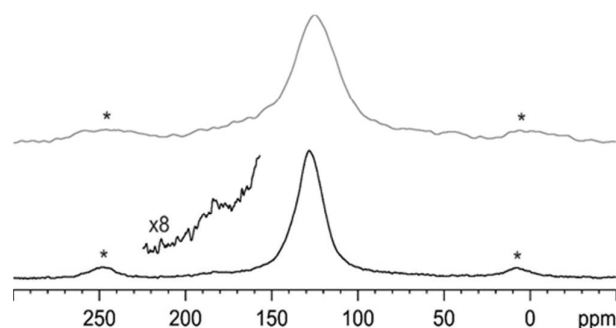


Fig. 3. ^{13}C (100.65 MHz) CPMAS NMR spectra of C_W (grey) and C_Chemical (black) recorded at 12 kHz. Asterisks denote spinning sidebands. The inset shows a magnification of the region characteristic of $\text{C}=\text{O}$ functional groups.

position is characteristic of $\text{C}=\text{O}$ functional groups. A similar trend is observed also in the ^1H MAS spectra (Fig. S3). They are characterized by a single broad resonance around 5.5 ppm, with that of C_W (FWHM 5600 Hz) broader than that of C_Chemical (FWHM 2850 Hz).

3.3.3 Raman spectroscopy. Fig. 4 shows the Raman spectra of both C_W and C_Chemical carbons collected with an excitation λ of 514 nm, whereas Fig. S4 reports the Raman spectra collected with a λ of 244 nm. The former give information mainly on the microcrystalline graphitic domains, because the green laser light has a strong selectivity towards the π states of sp^2 -hybridized carbon species.⁴⁸ On the contrary, UV Raman spectroscopy excites both the π and the σ states and hence it is able to probe both the sp^2 and sp^3 carbon species.⁴⁹

The two Raman spectra shown in Fig. 4 are both dominated by two intense bands, which are attributed to vibrational modes involving sp^2 -bonded carbon atoms belonging to disordered microcrystalline domains. In particular, the band centred at 1605 cm^{-1} (G band) is commonly assigned to the bond stretching of pairs of sp^2 carbon atoms (either in aromatic rings or chains),¹⁻³ as

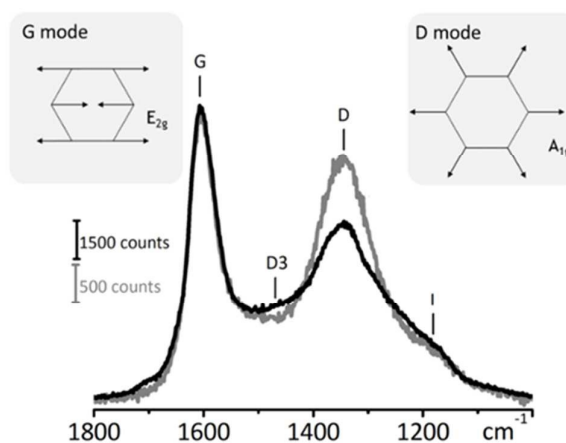


Fig. 4. Raman spectra of C_W (grey) and C_Chemical (black) carbons (counts as a function of the Raman shift in cm^{-1}), collected with an excitation $\lambda = 514\text{ nm}$, and assignment of the main bands. The insets show a scheme of the vibrational modes associated with the two main bands.

schematically shown in the left inset of Fig. 4. For crystalline graphite, the G mode has E_{2g} symmetry and gives a band at about 1580 cm^{-1} . The large shift observed in the present case is common to other disordered graphitic systems and has been explained by considering the overlap of a second band (D2, around 1620 cm^{-1}), which is ascribed to lattice vibrations analogous to that of the G band but involving surface graphene layers, i.e. not sandwiched between two other layers.⁵⁰⁻⁵⁴ Very recently, it has been reported that the C-C stretch Raman fingerprint systematically moves to higher frequency whenever the graphitic molecular nanostructure goes from a planar geometry to a strained geometry.⁵⁵ On these basis, the position of the G band in the present spectra provides an evidence that the graphene stacking order is very low in both carbons, in agreement with XRPD data, and that the graphene layers are at least partially defective.

On the other hand, the origin of the band close to 1350 cm^{-1} (band D, or D1 in the specialized literature) has been debated for long time; it is usually assigned to a lattice breathing mode with A_{1g} symmetry (right inset of Fig. 4), which is forbidden in ideal graphitic crystals, but becomes Raman active in presence of structural disorder,^{1-3,53,54,56} although the theoretical work of Thomsen and Reich ascribes it to a double resonant Raman scattering.⁵⁷ In particular, it has been suggested to arise from carbon atoms close to the edge of a graphene layer. Hence, the relative ratio between the intensity of the G and D bands - $I(\text{D})/I(\text{G})$ - should correlate with the degree of structural disorder. After the first report of Tuinstra and Koenig,⁵⁸ who reported that the intensity ratio between the two bands varies inversely with carbon cluster dimension (TK correlation), the $I(\text{D})/I(\text{G})$ value has long been indicative of the size of the graphitic domains in different carbon-based materials. Nevertheless, the extraction of the $I(\text{D})/I(\text{G})$ ratio from the Raman spectra is ambiguous in literature and large discrepancies are found according to the different evaluation techniques of the Raman spectra. More recently it has been argued that the TK correlation is not applicable for graphitic

domains having lateral dimension smaller than about 2 nm. The argument is based on the fact that the intensity of the D band is proportional to the probability of finding a six-fold ring in the cluster, which is proportional to the cluster area. Therefore, for crystallite sizes below 2 nm the development of a D band in the Raman spectrum indicates ordering, which is exactly the opposite as for graphitic clusters larger than 2 nm.⁵⁹ It is thus clear that the correlation of the I(D)/I(G) value with structural properties of carbons is not straightforward. In the present case, the Raman spectra of C_W and C_{Chem} carbons are clearly characterized by a different I(D)/I(G), being the value higher for C_W than for C_{Chem} . According to the XRPD data discussed above, both carbons are characterized by graphitic domains smaller than 2 nm and are more extended for C_W than for C_{Chem} . In these conditions the TK correlation is no more valid and the higher I(D)/I(G) value for C_W indicates that it is characterized by more ordered sp^2 domains with respect to C_{Chem} .

Additional broad absorptions are observed in the Raman spectra of both carbons, around 1450 cm^{-1} (D3 band, in between the G and D bands), attributed to a statistical distribution of amorphous carbon on interstitial position of the graphitic islands,⁶⁰ and around 1150 cm^{-1} (I band), originated from a coexistence of sp^3 and sp^2 phases (the last one under the form of conjugated non-aromatic polyenes).⁶¹ Both of them have been attributed to stretching vibrations involving the amorphous carbon phase. These bands are relatively more prominent for C_{Chem} , suggesting that the fraction of amorphous carbon is larger than in C_W . Finally, in the spectrum of C_{Chem} a weak, but well resolved, band is observed around 1700 cm^{-1} , which indicates the presence of C=O groups.⁶² This observation is in good agreement with the ^{13}C CPMAS SSNMR measurements, and confirms that C_{Chem} contains a larger amount of surface oxygen-containing groups.

3.4 Surface properties of C_W and C_{Chem} and functional groups

With the aim to investigate in detail the surface properties of the two activated carbons at a molecular level we carried out a thorough investigation by means of three techniques which are sensitive to the surface species: XPS, DRIFT and INS spectroscopy.

3.4.1 XPS spectroscopy. High-resolution XPS spectra of C 1s excitation for both C_W and C_{Chem} showed a complex envelope, indicative of several carbon species at the carbon surface. For both carbons the spectra were deconvoluted into six Gaussian components as reported in Table S2 and Table S3 and shown in Fig. 5. The most intense band (Peak B), located around 284.7 eV and presenting an asymmetric tail at high binding energies (BEs), is assigned to graphitic sp^2 carbon.⁶³ The other bands witness the presence of several C-O bonds.⁶³ In particular, peak C is usually assigned to carbon species in alcohol (C-OH) or ether (C-O-C) groups; peak D to carbon in carbonyl groups; and peak E to carboxyl and/or ester groups. Finally, band F is a satellite peak of shake-up type due to $\pi-\pi^*$ transitions in aromatic rings.¹⁷

The relative atomic concentration O/C in C_{Chem} is about the double of that in C_W , indicating that the surface of C_{Chem} is more oxidized than that of C_W . As a consequence, the main C 1s band (band B) appears narrower in the spectrum of C_W than in C_{Chem} . Table S4 compares the relative amount of the different oxygenated species, as obtained by normalizing the area of the six deconvoluted bands in the XPS spectra to the area of peak B, set arbitrarily to 100. In both carbons, the most abundant oxygenated species are C-OH or C-O-C (band C).

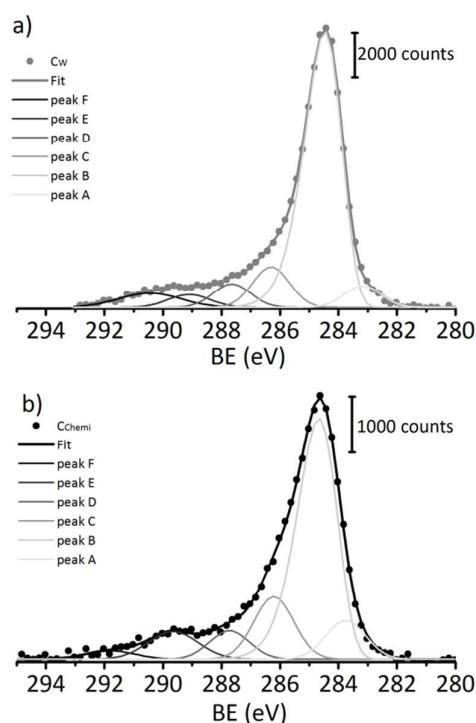


Fig. 5. High-resolution XPS spectra of C 1s peak for C_W and C_{Chem} and corresponding fits with six Gaussian components. For details see Table S2 and Table S3.

3.4.2 DRIFT spectroscopy. IR spectroscopy has been widely used to characterize the surface species in different carbon-based materials,¹⁻³ including coals, carbon blacks, chars, carbon films,^{64,65} activated carbons,⁶⁶⁻⁷³ and carbon-supported metal nanoparticles.^{31,32} In general, IR spectra of carbon materials are difficult to obtain because of problems in sample preparation, poor transmission, and uneven light scattering. More important, the electronic structure of carbon materials results in a complete absorption band through the visible region and the infrared one, which limits the collection of the spectra in the conventional transmission mode. For these reasons, very often IR spectra of carbon-based materials are characterized by unavoidable spectral artefacts or distortions, which complicate the data interpretation. At least part of the problem can be avoided by performing the measurements in diffuse reflectance mode. Fig. 6 shows the DRIFT spectra of C_W and C_{Chem} in the $2000 - 600\text{ cm}^{-1}$ region. The two spectra are characterized by the same main absorption bands, although

the total intensity of the spectra is around one order of magnitude larger for $C_{\text{Chem}}^{\text{Chem}}$.

The assignment of the main absorption bands is not trivial, also because several discrepancies are present in literature. However, the following assignments seem now firmly established:

- i) The narrow and prominent absorption band centred around 1600 cm^{-1} , whose assignment has been controversial for a long time, is assigned to $\nu(\text{C}=\text{C})$ vibrational modes of conjugated sp^2 bonds belonging to graphitic islands.⁷⁴ The

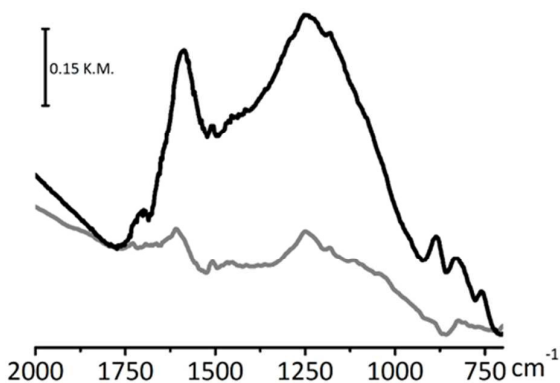


Fig. 6. DRIFT spectra of C_w (grey) and C_{Chem} (black) carbons (Kubelka-Munk units as a function of the wavenumber in cm^{-1}). The spectra were collected in air, using powdered samples and without dilution.

intensity of this band would be reinforced by the presence of oxygen atoms, most likely because of an increase in the dipole moment associated with these ring vibrations. This band is more intense in the spectrum of C_{Chem} that, according to Raman, XPS and ^{13}C SSNMR data, contains a larger amount of oxygenated species.

- ii) The intense and very broad absorption in the $1300 - 1000\text{ cm}^{-1}$ region is due to the overlap of many absorption bands difficult to be distinguished and due to many vibrational modes. In-plane C-H bending modes should contribute in this region,⁷⁴ but they are necessarily strongly coupled with the collective modes of the carbonaceous C-C skeleton, whose frequency range increases with the size of the system. This is the case not only for the C-H vibration, but also for any other modes associated to geometrical distortion of the C-C skeleton.⁷⁵ This is the main reason why no specific absorption bands are observed in this frequency range. In addition, most of the oxygenated species detected by XPS may give absorption in this region. Finally, it is important to notice that the P=O stretching vibration of phosphonate groups, which have been detected on C_{Chem} sample by ^{31}P CPMAS SSNMR technique, should also contribute in this region ($1380-1140\text{ cm}^{-1}$).⁷⁶ Although it is not possible to exclude that a fraction of the total absorbance in the $1300 - 1000\text{ cm}^{-1}$ region for C_{Chem} is due to the presence of surface phosphonates, we are inclined to exclude that this is the main reason for the much higher intensity of the DRIFT spectrum of C_{Chem} sample.
- iii) The series of narrow bands in the $900-750\text{ cm}^{-1}$ range is characteristic of the IR spectra of many molecules consisting

of several condensed rings, and are assigned to the out-of-plane vibrations of C-H bonds of condensed rings edges.⁷⁵ It has been demonstrated that the frequencies of the C-H deformational modes of aromatic species are dependent on the number of adjacent hydrogen atoms. According to the nomenclature proposed by Zander, for substituted benzenes the following values were reported: $860-910\text{ cm}^{-1}$ for an isolated hydrogen atom (*solo*), $800-810\text{ cm}^{-1}$ and $810-860\text{ cm}^{-1}$ for two adjacent hydrogen atoms (*duo*), and $750-770\text{ cm}^{-1}$, $770-800\text{ cm}^{-1}$ and $800-810\text{ cm}^{-1}$ for three adjacent hydrogen atoms (*trio*). In the spectrum of C_{Chem} sample three well defined bands are observed at 880 cm^{-1} (*solo*), $838 - 807\text{ cm}^{-1}$ (*duo + trio*) and 758 cm^{-1} (*trio*), which suggest a large heterogeneity of boundaries. The absorption bands due to C-H out-of-plane vibrations are definitely less intense in the spectrum of C_w , as expected because of the larger size of the sp^2 domains.

- iv) Finally, in the spectrum of C_{Chem} a weak but well defined absorption band is observed at 1707 cm^{-1} , which is assigned to $\nu(\text{C}=\text{O})$ vibrational mode, in good agreement with ^{13}C CPMAS NMR, Raman and XPS data.

Summarizing, the DRIFT spectra shown in Fig. 6 demonstrate that the surface properties of C_w are mainly dictated by terminal C-H bonds, while in C_{Chem} a detectable amount of C=O functional groups are clearly identified. The presence of these oxygen-containing surface species (and of others, not easily identified by FT-IR but detected by XPS), as well as the reduced dimension of the sp^2 islands (as revealed by the previously discussed techniques), might be the main causes for the much higher intensity of the whole DRIFT spectrum for C_{Chem} than for C_w . Indeed, an increase dipole moment associated with the sp^2 ring vibrations is expected in the presence of defect sites, including heteroatoms and islands terminations.

3.4.3 INS spectroscopy. Inelastic neutron scattering technique has been widely used for detailed studies on carbon-based materials and carbon-supported catalysts.⁷⁷⁻⁸³ This technique is extremely powerful in detecting vibrations involving the terminating hydrogen atoms at the edges of the sp^2 domains. Fig. 7 shows the INS spectra of C_w and C_{Chem} carbons. The spectra were normalized to the sample mass and to the proton current of the source, integrated along the acquisition time, so that the intensity of each band is directly proportional to the amount of the corresponding species.

All the bands observed in the spectra are due to vibrational modes that involve significant hydrogen displacement, since the neutron cross-section for the hydrogen nucleus is one order of magnitude higher than that of all the other elements. The two spectra are very similar, although the total intensity is almost two times higher for C_{Chem} than for C_w . This means that the type of hydrogen terminations and their relative abundance are basically the same in the two carbons, but more abundant in C_{Chem} than in C_w . The larger amount of hydrogen termination in C_{Chem} sample is only partially explained in terms of the higher surface area, which would account only for a factor 1.5. Hence, we should conclude that in C_{Chem} carbon the sp^2 domains are smaller than in C_w , in

good agreement with previously discussed results. However, it is worth to notice that discrepancies between the intensity of the INS spectra and hydrogen content in carbon materials have been reported in the past. In particular, Fillaux et al.⁷⁷⁻⁸³ suggested that a part of the hydrogen species in carbons behave like free protons and therefore they respond in a different way. A clear explanation of this phenomenon is still not available.

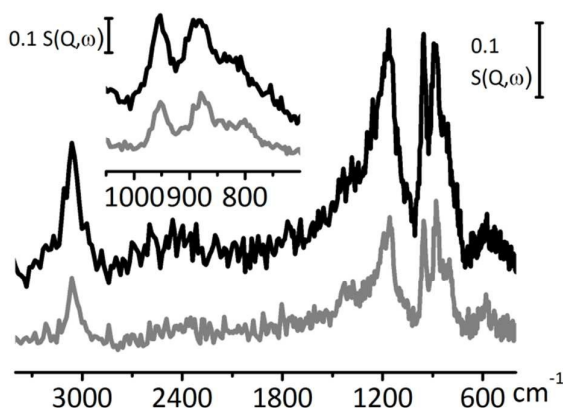


Fig. 7. Incoming proton current and mass normalised INS spectra of C_w (grey) and C_{Chemis} (black) carbons ($S(Q, \omega)$) as a function of the energy transfer in cm^{-1} . The inset shows a magnification of the $1050 - 600 \text{ cm}^{-1}$ range.

The absorption band centred around 3060 cm^{-1} is assigned to $\nu(\text{C-H})$ vibrational modes of aromatic species. At the other extreme of the spectra, the weak bands in the $700 - 400 \text{ cm}^{-1}$ region are mainly due to C-C torsion modes of the carbon atoms at the edge of the fragment, which indirectly cause a substantial movement of the hydrogen atoms (riding vibrations).⁸³ It is worth noticing that also COOH functional groups may weakly contribute in this vibrational region.⁸³ The broad bands around 1200 cm^{-1} and in the $800 - 1000 \text{ cm}^{-1}$ region are due to the in-plane and out-of-plane C-H bending modes of hydrogen species belonging to condensed rings edges.⁷⁸ In particular, in the latter region the most prominent bands are observed at $952, 880, 830, 800$ and 760 cm^{-1} . Most of these bands coincide with those observed in the DRIFT spectra and assigned in terms of *solo*, *duo* and *trio* structures. In particular, according to literature⁷⁸ and to our recent calculations,⁸³ the most intense band at 880 cm^{-1} is associated to CH out-of-plane vibrations of *solo* species which vibrate in phase; hence, it is indicative of extended sp^2 domains having regular borders. Curiously, the intense band at 952 cm^{-1} is absent in the DRIFT spectra and it was rarely commented in literature. Very recently we have proposed an assignment in terms of CH out-of-plane mode of *duo*, *trio* and *quatro* species vibrating not in phase;⁸³ thus, this band is associated with irregular borders of sp^2 domains. The relative intensity of this band with respect to that at 880 cm^{-1} is greater for C_{Chemis} , indicating that the sp^2 domains in C_{Chemis} present less extended and more defective borders.

In summary, INS measurements allowed the full characterization of the hydrogen terminations at the sp^2

domains. It was found that the hydrogen content is about the double in C_{Chemis} , that means that the average size of the graphitic plates is smaller in C_{Chemis} . Moreover, the distribution of the hydrogen termination is similar but not the same in the two carbons, and in particular C_{Chemis} presents less extended and more irregular borders.

3.4.4 Vibrational properties of C_w and C_{Chemis} : a comparison between Raman, DRIFT and INS spectra.

In this section we will briefly comment on the complementarity of the Raman, DRIFT and INS techniques. To facilitate the comparison, Fig. S5 shows again the Raman, DRIFT and INS spectra of the C_{Chemis} carbon plotted in the same $1900 - 500 \text{ cm}^{-1}$ wavenumber region, where the most characteristic bands appear. Table 3 summarizes the main bands observed in the three spectra and the corresponding assignment. In order for a vibrational mode in a molecule (or a molecular fragment) to be IR or Raman active, it must be associated with changes in the dipole moment or in the polarizability, respectively. The Raman spectrum of C_{Chemis} (and of a carbon in general) is dominated by $\nu(\text{C=C})$ stretching modes involving pairs or rings of sp^2 carbons, i.e. collective modes which are strongly related to the structural order of the sp^2 domains (G and D bands in Table 3). Hence, Raman spectra convey structural information mainly on the bulk phase of carbon materials, while surface functional groups are rarely observed.

On the contrary, the $\nu(\text{C=C})$ vibrational modes of conjugated double bonds in graphitic sp^2 domains are observed in the IR spectrum of a carbon only in the presence of defects (surface terminations, heteroatoms, functional groups, radical carbon species and others), which are responsible for an increase of the dipole moment associated with the rings vibrations. Consequently, IR spectra bring only indirect information on the bulk properties of carbon-based materials, while they contain direct information on the surface species, including both the C-H groups at the periphery of sp^2 clusters (usually characterized by weak absorptions) and functional groups containing hetero-atoms such as oxygen (generally giving more intense absorption bands, depending on the specific extinction coefficient).

In carbons hydrogen content is limited just to the surface (either in the terminal C-H species or in oxygen-containing functional groups). This makes INS a technique extremely sensitive to surface species. Most of the bands observed in the INS spectrum of C_{Chemis} are also found in the DRIFT spectrum, with a few important differences: i) in the INS spectrum the bands are generally narrower and much more resolved; ii) INS spectra are not subjected to selection rules and then show more bands.

Summarizing, among the three vibrational techniques Raman spectroscopy (excitation $\lambda = 514 \text{ nm}$) is the only one that gives direct information on the bulk properties of carbons and structural information on the sp^2 domains can be derived provided that XRPD data are available. DRIFT spectroscopy is the technique of choice to qualitatively investigate the

presence of functional groups that are usually characterized by high extinction coefficients. However, in some cases different IR absorption bands can overlap, making the interpretation of the spectra difficult; in these cases, coupling FT-IR

spectroscopy with XPS might be beneficial for understanding. INS spectroscopy (on carefully dehydrated samples) is definitely the best technique to obtain qualitative and

Table 3. Summary of the observed bands (in cm^{-1}) in Raman ($\lambda = 514 \text{ nm}$), DRIFT and INS spectra of C_{chemi} carbon, and corresponding assignment.

RAMAN		DRIFT		INS	
Bands (cm^{-1})	Assignment	Bands (cm^{-1})	Assignment	Bands (cm^{-1})	Assignment
1700 (vw)	v(C=O) G band	1707	v(C=O)		
1605	v(C=C) of pairs of sp^2 C atoms D3 band	1600	v(C=C) of sp^2 C atoms (enhanced by defects)		
1500 (br)	Amorphous phase D band				
1350 (br)	v(C=C) of sp^2 C atoms close to the edge I band	1300-1100 (br)	C-H in-plane bending + collective modes of the C-C skeleton + vibration of oxygenated groups	1200	C-H in-plane bending
1200 (w)	Amorphous phase			956 (s)	C-H out-of-plane of duo and trio at irregular borders
		880 (w)	C-H out-of-plane of solo	880 (s)	C-H out-of-plane of solo at extended borders
		838-807 (w)	C-H out-of-plane of duo and trio	830	C-H out-of-plane of duo and trio
		758 (w)	C-H out-of-plane of duo and trio	760	C-H out-of-plane of duo and trio

vw = very weak; w = weak; br = broad; s = strong.

quantitative information on the C-H terminations of the sp^2 domains, although it is scarcely informative on the presence of other functional groups. It comes out that the synergic coupling of the three techniques is fundamental to extract from vibrational data also information on the structural properties of activated carbons at a molecular scale.

In order to definitely validate our findings, we have treated the C_{chemi} carbon at $750 \text{ }^\circ\text{C}$ in inert atmosphere, and successively measured the Raman, DRIFT and INS spectra, as shown in Fig. S5 (light grey). In all the three cases, the spectra of the sample treated at high temperature decrease in intensity and become very similar to those of the C_w carbon discussed previously. From the discussion above, the much larger intensity of the vibrational spectra of C_{chemi} with respect to C_w is attributed to the presence of smaller and more defective sp^2 domains in C_{chemi} carbon. Hence, the decrease of the overall spectral intensity upon treatment at high temperature provides evidence that C_{chemi} undergoes a graphitization process. Additional discussion can be found in Section S5.

3.5 Vibrational properties of Pd/C catalysts

Raman, DRIFT and INS spectroscopies were applied to investigate the Pd/ C_w and Pd/ C_{chemi} catalysts, with the aim to evaluate if the catalyst preparation has an influence on the properties of the carbon support. Indeed, during the catalyst synthesis the original support may undergo modifications at the nano- and micro-scale level,⁹ although this is often neglected. Preparation of the Pd/C catalysts involves metal deposition in a basic medium, washing, and thermal treatments. In these conditions, activated carbons can release

ashes (that can be washed out or can re-precipitate inside the pores),¹⁰ may undergo a partial reconstruction involving defective sp^2 domains, and a modification of the surface functional groups may also occur. In turn, the modifications of the carbon support during the catalyst preparation may influence its activity towards reactants and products, and can affect the availability of the metal particles during the catalytic process.

In a previous work we demonstrated that activated carbons are quite inert toward deposition-precipitation of the active metal phase: only very small variations of surface area and pore volume were observed,⁹ indicating that catalyst's preparation does not involve a large reconstruction of the supports. This is confirmed by the similarity of the Raman spectrum of Pd/ C_w with that of the pristine C_w support, as shown in Fig. 8a, although a slight increase of the absorption band around 1500 cm^{-1} suggests that in Pd/ C_w the fraction of amorphous carbon is slightly higher than in C_w . Also the DRIFT spectrum of Pd/ C_w is very similar to that of C_w (Fig. 8b), excluding that during catalyst's preparation new functional groups are formed at the carbon surface. Finally, in the INS spectrum of Pd/ C_w the bands associated with C-H out-of-plane vibrations are slightly less intense than for bare C_w (Fig. 8c), indicating that a minority of the C-H terminations are involved in the deposition of the active phase. In particular, the band at 880 cm^{-1} , indicative of regular borders, is the most affected one. A similar behaviour was observed for Pd/ C_{chemi} .

The results shown in Fig. 8 demonstrate that the structural and surface properties of Pd/C catalyst are basically the same as those of the pristine carbons. Hence, a comprehensive characterization of the activated carbons with a multi-

technique approach as proposed in this work gives all the information useful to tailor the catalyst for a specific purpose.

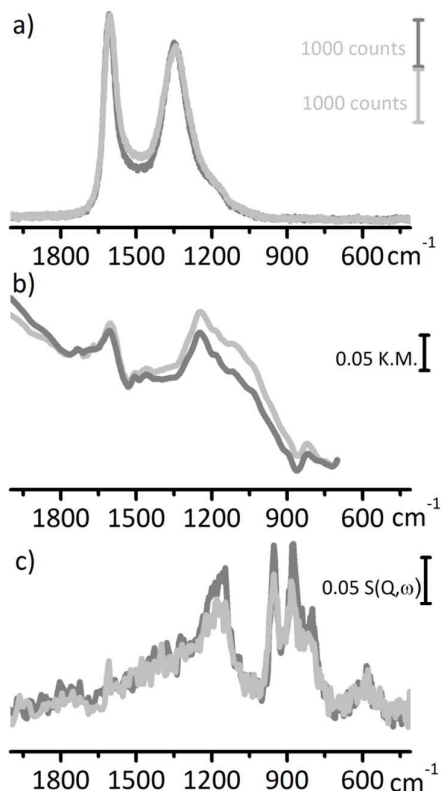


Fig. 8. Raman ($\lambda = 514$ nm, part a), DRIFT (part b) and INS (part c) spectra of C_w (dark grey) and of the corresponding Pd/C_w catalyst (light grey).

4. Conclusions

Two couples of Pd/C catalysts, characterized by the same metal dispersion but a different carbon support (C_w and C_{chemi}), were tested in two hydrogenation reactions. We found that the catalytic performances strongly depend on the nature of the support. The two carbons were obtained from the same raw material, but activated in the presence of either steam or phosphoric acid. Hence, the activation procedure of the carbons has a relevant consequence on the performances of the catalysts. To understand the origin of this effect, we underwent a comprehensive and systematic characterization of the two carbons and of the Pd/C catalysts by a multitude of techniques with different sensitivity and selection rules.

We were able to fully understand how the activation procedure influences the morphology, the composition, the texture, the structure and the surface properties of the two activated carbons, both at a micro- and at the nanoscale. In particular, it was found that activation in the presence of phosphoric acid leads to the formation of micro-particles smaller than those obtained in the presence of steam. The micro-structure is reflected at a nano-scale: both carbons are mainly graphitic in nature, but C_{chemi} is constituted by graphitic

domains smaller than C_w . The sp^2 domains have a similar morphology in the two carbons, although in C_{chemi} they are more uniform in size. The surface properties of both activated carbons are determined by terminal C-H bonds and by oxygenated species. The distribution of the hydrogen termination is similar but not the same in the two carbons, and in particular C_{chemi} presents less extended and more irregular borders. C_{chemi} contains more oxygenated species, mainly carbonyl (C=O) and ethers (C-O-C), which contribute in increasing the dipole moment associated with the sp^2 ring vibrations and in rendering the whole surface more polar. Finally, C_{chemi} comprises also a detectable amount of phosphorous (at least partially grafted to the carbon in the form of phosphonate species), which is however localized in the bulk and not at the surface, and hence is not relevant for catalysis.

The comprehensive characterization approach proposed in this work allows to rationalize, at least in part, the role of activated carbons in enhancing the performances of a hydrogenation catalyst. Pd/C_w is more selective than Pd/C_{chemi} in the transfer hydrogenation of resorcinol to 1,3-cyclohexanedione. It is a current opinion that during hydrogenation of an aromatic ring over a heterogeneous catalyst (as for the hydrogenation of resorcinol) the hydrogen molecule is split into hydrogen atoms over the metal active phase, while aromatic substrates are adsorbed onto the supports mainly through hydrogen bonds and electrostatic effects.^{84,85} The adsorbed aromatic ring is then attacked by the adsorbed hydrogen atoms and the hydrogenation reaction occurs. Selectivity is promoted when the product of interest (1,3-cyclohexanedione in our case) is desorbed from the support before undergoing a successive hydrogenation. It is expected that the adsorption of resorcinol onto the carbon support (which is the preliminary step to its hydrogenation) is favoured in presence of regular sp^2 domains. The results discussed in this work demonstrate that C_w has larger and more regular sp^2 domains than C_{chemi} , and hence correlate the structure of the carbon with the better catalytic performances in the transfer hydrogenation of resorcinol to 1,3-cyclohexanedione. A similar effect was recently reported for a graphene-supported Pd catalyst, which displays an excellent selectivity in the same reaction due to the giant π -conjugate interactions between the graphene nano-sheet and the benzene ring of resorcinol.⁸⁶

On the other hand, the regularity of the sp^2 domains in the carbon support is not required for selective catalytic debenzilation reactions, where a high activity for hydrogenolysis should be combined with a low tendency for the reduction of the aromatic rings. In this class of reactions the polarity of the reaction medium is more important, and indeed debenzilation reactions very often are carried out in alcoholic solvents or in acetic acid.^{22,24} On these basis, it is not surprising that C_{chemi} (which has a more polar and irregular surface, with a larger amount of surface functional groups, as demonstrated in this work) performs better than C_w in the debenzilation of ethyl-benzyl-aniline.

Acknowledgements

We sincerely thank our colleagues and friends Francesca Bonino and Matteo Signorile for the helpful discussion on the Raman spectra, and Ettore Vittone for the discussion on the XPS measurements. C.L. is grateful for support from the Mega-grant of the Russian Federation Government to support scientific research at the Southern Federal University, No. 14.Y26.31.0001.

Notes and references

- K.-D. Henning and H. von Kienle, *Carbon*, 5. *Activated Carbon*, in: Ullmann's Encyclopedia of Industrial Chemistry; Wiley-VCH, **2010**.
- R. Schlogl, 2.3.15 *Carbons*, in: Handbook of heterogeneous catalysis; Ertl, G.; Knozinger, H.; Schuth, F.; Weitkamp, J., Ed.; Wiley-VCH, **2008**; Vol. 1, p. 357.
- H. Marsh and F. Rodriguez-Reinoso, in: *Activated carbon*; Elsevier, **2006**, p. 13.
- A. Ahmadpour and D. D. Do, *Carbon* 1996, **34**, 471.
- B. S. Girgis, S. S. Yunis and A. M. Soliman, *Mater. Lett.* 2002, **57**, 164.
- H. Marsh and P. L. Walker Jr, *Fuel Process. Technol.* 1979, **2**, 61.
- H. Marsh, D. S. Yan, T. M. O'Grady and A. Wennerberg, *Carbon* 1984, **22**, 603.
- R. Rodrigues, M. Gonçalves, D. Mandelli, P. P. Pescarmona and W. A. Carvalho, *Catalysis Science and Technology* 2014, **4**, 2293.
- R. Pellegrini, G. Leofanti, G. Agostini, E. Groppo, M. Rivallan and C. Lamberti, *Langmuir* 2009, **25**, 6476.
- E. J. A. X. Van De Sandt, A. Wiersma, M. Makkee, H. Van Bekkum and J. A. Moulijn, *Applied Catalysis A: General* 1998, **173**, 161.
- A. Wiersma, E. J. A. X. Van De Sandt, M. A. Den Hollander, H. Van Bekkum, M. Makkee and J. A. Moulijn, *Journal of Catalysis* 1998, **177**, 29.
- L. Faba, E. Díaz and S. Ordóñez, *Catalysis Science and Technology* 2015, **5**, 1473.
- M. Galhetas, M. A. Andrade, A. S. Mestre, E. Kangni-Foli, M. J. Villa De Brito, M. L. Pinto, H. Lopes and A. P. Carvalho, *Physical Chemistry Chemical Physics* 2015, **17**, 12340.
- H. Teng, T.-S. Yeh and L.-Y. Hsu, *Carbon* 1998, **36**, 1387.
- J. Laine and S. Yunes, *Carbon* 1992, **30**, 601.
- G. A. Zickler, B. Smarsly, N. Gierlinger, H. Peterlik and O. Paris, *Carbon* 2006, **44**, 3239.
- S. Biniak, G. Szymański, J. Siedlewski and A. Świtkowski, *Carbon* 1997, **35**, 1799.
- J. L. Figueiredo, M. F. R. Pereira, M. M. A. Freitas and J. J. M. Órfão, *Carbon* 1999, **37**, 1379.
- <http://www.chimet.com/en/catalyst>.
- G. Agostini, C. Lamberti, R. Pellegrini, G. Leofanti, F. Giannici, A. Longo and E. Groppo, *ACS Catal.* 2014, **4**, 187.
- R. A. W. Johnstone and A. H. Wilby, *Chem. Rev.* 1985, 129.
- H.-U. Blaser, A. Indolese, A. Schnyder, H. Steiner and M. Studer, *J. Mol. Catal. A: Chem.* 2001, **173**, 3.
- V. Elango and S. Rajagopal, **1998**, United States Patent 5,744,648.
- K. G. Griffin, S. Hawker and M. A. Batti, in: *Catalysis of organic Reactions*; Malz, R. E., Ed.; Marcel Dekker, Inc.: New York, **1996**, p. 325.
- R. Pellegrini, G. Agostini, E. Groppo, A. Piovano, G. Leofanti and C. Lamberti, *Journal of Catalysis* 2011, **280**, 150.
- D. Colognesi, M. Celli, F. Cilloco, R. J. Newport, S. F. Parker, V. Rossi-Albertini, F. Sacchetti, J. Tomkinson and M. Zoppi, *Appl. Phys. A* 2002, **74**, S64.
- O. Arnold, J. C. Bilheux, J. M. Borreguero, A. Buts, S. I. Campbell, L. Chapon, M. Doucet, N. Draper, R. Ferraz Leal, M. A. Gigg, V. E. Lynch, A. Markvardsen, D. J. Mikkelsen, R. L. Mikkelsen, R. Miller, K. Palmen, P. Parker, G. Passos, T. G. Perring, P. F. Peterson, S. Ren, M. A. Reuter, A. T. Savici, J. W. Taylor, R. J. Taylor, R. Tolchenov, W. Zhou and J. Zikovsky, *Nucl. Instrum. Methods Phys. Res., Sect. A* 2014, **764**, 156.
- J. R. Anderson and K. C. Pratt, in: *Introduction to Characterization and Testing of Catalysts*; Academic Press: Sydney, Australia, **1986**, p. 1.
- G. Agostini, R. Pellegrini, G. Leofanti, L. Bertinetti, S. Bertarione, E. Groppo, A. Zecchina and C. Lamberti, *J. Phys. Chem. C* 2009, **113**, 10485.
- G. Prelazzi, M. Cerboni and G. Leofanti, *J. Catal.* 1999, **181**, 73.
- J. J. Venter and M. A. Vannice, *Inorg. Chem.* 1989, **28**, 1634.
- G. Gokagac, J. M. Leger and F. Hahn, *Z. Naturforsch. B* 2003, **58**, 423.
- S. Bertarione, C. Prestipino, E. Groppo, D. Scarano, G. Spoto, A. Zecchina, R. Pellegrini, G. Leofanti and C. Lamberti, *Physical Chemistry Chemical Physics* 2006, **8**, 3676.
- H. Benaddi, D. Legras, J. N. Rouzaud and F. Beguin, *Carbon* 1998, **36**, 306.
- T. Budinova, E. Ekinci, F. Yardim, A. Grimm, E. Björnbo, V. Minkova and M. Goranova, *Fuel Process. Technol.* 2006, **87**, 899.
- A. M. Puziy, O. I. Poddubnaya, A. Martínez-Alonso, F. Suárez-García and J. M. D. Tascón, *Carbon* 2002, **40**, 1493.
- A. M. Puziy, O. I. Poddubnaya, R. P. Socha, J. Gurgul and M. Wisniewski, *Carbon* 2008, **46**, 2113.
- H. Fujimoto, *Carbon* 2003, **41**, 1585.
- C. R. Houška and B. E. Warren, *J. Appl. Phys.* 1954, **25**, 1503.
- Z. Q. Li, C. J. Lu, Z. P. Xia, Y. Zhou and Z. Luo, *Carbon* 2007, **45**, 1686.
- T. D. Shen, W. Q. Ge, K. Y. Wang, M. X. Quan, J. T. Wang, W. D. Wei and C. C. Koch, *Nanostruct. Mater.* 1996, **7**, 393.
- A. Cuesta, P. Dhameincourt, J. Laureyns, A. Martínez-Alonso and J. M. D. Tascón, *J. Mater. Chem.* 1998, **8**, 2875.
- C. A. Johnson, J. W. Patrick and K. Mark Thomas, *Fuel* 1986, **65**, 1284.
- T. Ungár, J. Gubicza, G. Ribárik, C. Pantea and T. W. Zerda, *Carbon* 2002, **40**, 929.
- R. K. Harris, in: *Encyclopedia of Magnetic Resonance*; Wasylishen, R. E.; Ashbrook, S. E.; Wimperis, S., Ed.; John Wiley & Sons Ltd, **2012**; Vol. Chichester, UK, p. 857.
- R. K. Harris, R. E. Wasylishen and M. J. Duer, *NMR Crystallography*; John Wiley & Sons Ltd: Chichester, UK, **2009**.
- M. R. Chierotti and R. Gobetto, *CrystEngComm* 2013, **15**, 8599.
- N. Wada, P. J. Gaczi and S. A. Solin, *J. Non-Cryst. Solids* 1980, **35-36, Part 1**, 543.
- K. W. R. Gilkes, H. S. Sands, D. N. Batchelder, J. Robertson and W. I. Milne, *Appl. Phys. Lett.* 1997, **70**, 1980.
- A. Sadezky, H. Muckenhuber, H. Grothe, R. Niessner and U. Pöschl, *Carbon* 2005, **43**, 1731.
- Y. Wang, D. C. Alsmeyer and R. L. McCreery, *Chem. Mater.* 1990, **2**, 557.
- O. Beyssac, B. Goffé, J.-P. Petit, E. Froigneux, M. Moreau and J.-N. Rouzaud, *Spectrochim. Acta, Part A* 2003, **59**, 2267.
- C. Castiglioni, M. Tommasini and G. Zerbi, *Philos. Trans. R. Soc. London, Ser. A* 2004, **362**, 2425.
- M. Tommasini, C. Castiglioni, G. Zerbi, A. Barbon and M. Brustolon, *Chem. Phys. Lett.* 2011, **516**, 220.
- H. A. Galué, *Chem. Sci.* 2014, **5**, 2667.

- 56 A. C. Ferrari, *Solid State Commun.* 2007, **143**, 47.
- 57 C. Thomsen and S. Reich, *Phys. Rev. Lett.* 2000, **85**, 5214.
- 58 F. Tuinstra and J. L. Koenig, *J. Chem. Phys.* 1970, **53**, 1126.
- 59 A. C. Ferrari and J. Robertson, *Phys. Rev. B* 2000, **61**, 14095.
- 60 T. Jawhari, A. Roid and J. Casado, *Carbon* 1995, **33**, 1561.
- 61 A. C. Ferrari and J. Robertson, *Phys. Rev. B* 2001, **63**, 121405.
- 62 D. Lin-Vien, N. B. Colthup, W. G. Fateley and J. G. Grasselli, *The Handbook of Infrared and Raman Characteristic Frequencies of Organic Molecules*; Academic Press: London, UK, **1991**.
- 63 NIST X-ray Photoelectron Spectroscopy Database, <http://srdata.nist.gov/xps/>.
- 64 J. Zawadzki, B. Azambre, O. Heintz, A. Krztoń and J. Weber, *Carbon* 2000, **38**, 509.
- 65 J. Zawadzki and M. Wiśniewski, *Carbon* 2003, **41**, 2257.
- 66 D. B. Mawhinney and J. T. Yates Jr, *Carbon* 2001, **39**, 1167.
- 67 B. J. Meldrum and C. H. Rochester, *J. Chem. Soc., Faraday Trans.* 1990, **86**, 861.
- 68 B. J. Meldrum and C. H. Rochester, *J. Chem. Soc., Faraday Trans.* 1990, **86**, 1881.
- 69 B. J. Meldrum and C. H. Rochester, *J. Chem. Soc., Faraday Trans.* 1990, **86**, 2997.
- 70 B. J. Meldrum and C. H. Rochester, *J. Chem. Soc., Faraday Trans.* 1990, **86**, 3647.
- 71 C. Moreno-Castilla, F. Carrasco-Marín and A. Mueden, *Carbon* 1997, **35**, 1619.
- 72 C. Moreno-Castilla, M. A. Ferro-García, J. P. Joly, I. Bautista-Toledo, F. Carrasco-Marín and J. Rivera-Utrilla, *Langmuir* 1995, **11**, 4386.
- 73 C. Moreno-Castilla, N. V. López-Ramón and F. Carrasco-Marín, *Carbon* 2000, **38**, 1995.
- 74 A. C. Ferrari, S. E. Rodil and J. Robertson, *Phys. Rev. B* 2003, **67**, 155306.
- 75 A. Centrone, L. Brambilla, T. Renouard, L. Gherghel, C. Mathis, K. Müllen and G. Zerbi, *Carbon* 2005, **43**, 1593.
- 76 K. Nakamoto, *Infrared and Raman Spectra of Inorganic and Coordination Compounds*; John Wiley & Sons: New York, **1978**.
- 77 P. W. Albers, S. Bösing, H. Lansink Rotgerink, D. K. Ross and S. F. Parker, *Carbon* 2002, **40**, 1549.
- 78 P. W. Albers, J. Pietsch, J. Krauter and S. F. Parker, *Phys. Chem. Chem. Phys.* 2003, **5**, 1941.
- 79 F. Fillaux, R. Papoulet, S. M. Bennington and J. Tomkinson, *J. Non-Cryst. Solids* 1995, **188**, 161.
- 80 F. Fillaux, R. Papoulet, A. Lautié and J. Tomkinson, *Carbon* 1994, **32**, 1325.
- 81 F. Fillaux, R. Papoulet, A. Lautié and J. Tomkinson, *Fuel* 1995, **74**, 865.
- 82 P. J. R. Honeybone, R. J. Newport, J. K. Walters, W. S. Howells and J. Tomkinson, *Phys. Rev. B* 1994, **50**, 839.
- 83 A. Piovano, A. Lazzarini, R. Pellegrini, G. Leofanti, G. Agostini, S. Rudic, A. L. Bugaev, C. Lamberti and E. Groppo, *Adv. Cond. Matter Phys.* 2015, **2015**, 803267.
- 84 C. A. Hunter, *Chem. Soc. Rev.* 1994, **23**, 101.
- 85 C. A. Hunter, K. R. Lawson, J. Perkins and C. J. Urch, *J. Chem. Soc. Perkin Trans. 2* 2001, 651.
- 86 Z. Wei, R. Pan, Y. Hou, Y. Yang and Y. Liu, *Sci. Rep.* 2015, **5**, 15664.

